ELSEVIER

Contents lists available at ScienceDirect

Chemical Engineering Journal

journal homepage: www.elsevier.com/locate/cej





Percolating dynamic ion-conduction network in composite polymer electrolyte for high-performance lithium metal batteries

Xueying Yang ^a, Chenxi Sun ^b, Ruiyang Li ^b, Nanbiao Pei ^b, Xinyu Li ^a, Yi Deng ^a, Peng Zhang ^{a,*}, Jie Lin ^{c,*}, Jinbao Zhao ^{b,*}

- ^a College of Energy, Xiamen University, Xiamen 361102, PR China
- b State Key Laboratory of Physical Chemistry of Solid Surfaces, Collaborative Innovation Centre of Chemistry for Energy Materials, State-Province Joint Engineering Laboratory of Power Source Technology for New Energy Vehicle, Engineering Research Center of Electrochemical Technology, Minis try of Education, College of Chemistry and Chemical Engineering, Xiamen University, Xiamen 361005, PR China
- ^c School of Mechanical and Aerospace Engineering, Queen's University Belfast, Ashby Building, Stranmillis Road, Belfast BT9 5AH, UK

ARTICLE INFO

Keywords: PDOL Dynamic ion transport Li⁺ pathways Organic-organic interface

ABSTRACT

Solid polymer electrolytes are driving the development of solid-state lithium metal batteries due to their good interfacial compatibility and suitability for battery manufacturing processes. However, the widespread adoption of conventional solid polymer electrolytes is hindered by their slow ion transport kinetics. Here, a percolating dynamic ion-conducting network with PDOL@LLTO composite polymer electrolyte was developed by in-situ polymerization of DOL in the 3D scaffold of $Li_{0.33}La_{0.56}TiO_3$ nanofibers (LLTO NF). The LLTO NF resolves the critical issue of filler aggregation while providing a spatially-continuous inorganic framework for ion transport that lays the foundation for macroscopic dynamic ion percolation. The highly interconnected LLTO NF and its continuous PDOL-LLTO interface form ion transport pathways with low migration energy barriers, thereby alleviating the suppression of Li⁺ migration caused by the stable solvation structure in the polymer phase. Meanwhile, the remaining DOL weakens the stable solvated structure formed by the PDOL and establishes a charge-rich organic-inorganic interface, which further increases the dynamic characteristics of the ion transport network. With the synergistic organic-inorganic transport percolation network, therefore, PDOL@LLTO achieves exceptional Li⁺ transference number of 0.61 and ionic conductivity of $1.62 \times 10^{-4} \text{ S cm}^{-1}$. In addition, the improved solvated structure creates an inorganic-rich SEI on the anode, which further induced the uniform deposition of Li. The Li|PDOL@LLTO|Li symmetric cell exhibits outstanding cycling stability for 1000 h at 0.4 mA cm⁻², and the LFP|PDOL@LLTO|Li full cell achieved 94.6 % capacity retention after 100 cycles at 2C. Moreover, after 100 cycles, the Li|PDOL@LLTO|NCM811 full cell maintains remarkable capacity retention of 72 % at 1C, further demonstrating the long-term electrochemical stability and practical applicability of the PDOL@LLTO.

1. Introduction

Solid-State Lithium Metal Batteries (SSLMBs) are widely recognized as the next generation batteries owing to their intrinsic safety and superior energy density [1,2]. The solid-state electrolytes (SSEs), serving as both an electronic insulator and ionic conductor, critically govern the battery's charge/discharge kinetics and cycling stability. To ensure efficient battery operation, SSEs should possess minimal ionic resistance, facilitating fast and homogeneous lithium-ion diffusion [3]. Among various SSEs, solid polymer electrolytes (SPEs) exhibit promising

potential due to their inherent flexibility and excellent interfacial compatibility [4,5]. However, their critical electrochemical parameters, such as room temperature ionic conductivity ($\sigma < 10^{-5}~S~cm^{-1}$) and Li $^+$ transference number (t $_{\rm Li}^+ < 0.5$), remain inferior to those of liquid electrolytes, significantly limiting their application in high-performance SSLMBs [6,7].

Ion transport in SPEs primarily is governed by two fundamental processes: (i) the solvation of lithium salt by polar groups on the polymer chain, and (ii) ion migration via the dynamic rearrangement of polymer chain segments. Polyether-based SPEs, typified by poly

E-mail addresses: pengzhang@xmu.edu.cn (P. Zhang), j.lin@qub.ac.uk (J. Lin), jbzhao@xmu.edu.cn (J. Zhao).

^{*} Corresponding authors.

(ethylene oxide) (PEO), feature polar ether oxygen moieties (-C-O-C-) along their backbones [8]. These functional groups enable the formation of stable Li⁺ solvation structures, facilitating efficient lithium salts dissociation at the molecular level. However, this advantage also introduces critical challenges: firstly, the strong coordination between Li⁺ and the polymer chains creates a high desolvation energy barrier, fundamentally limiting Li⁺ mobility [9]. Secondly, Semi-crystalline polymers exhibit significant crystallinity at room temperature, which immobilizes chain segments and further impedes Li+ desolvation. Therefore, ionic conduction is confined to discrete amorphous domains, creating discontinuous transport pathways that prevent localized conductivity enhancements from translating into macroscopic, long-range ion conduction [10]. In contrast to the liquid electrolyte, where Li⁺ transport proceeds through solvation-shell-mediated vehicle diffusion, SPEs demonstrate restricted ion transport dynamics exhibiting frozen "static" ion transport behavior with both low ionic conductivity and diminished Li⁺ transference number due to such multiple interrelated factors [11].

To achieve rapid ion transport in SPEs, it is essential to simultaneously address the challenges by weakening the coordination between Li⁺ and polymer chains at the microscopic level while reducing crystallinity and enhancing chain segment mobility at the macroscopic level. Meanwhile, a complete and continuous ion transport network must be constructed throughout the whole polymer phase to mobilize ions otherwise restricted ion transport process and accelerate its kinetics [12,13]. In general, the introduction of organic additives (such as ionic liquids, plastic crystals, and diluents) can enable effective suppression of polymer crystallinity while simultaneously enhancing segmental dynamics, consequently facilitating improved ionic transport. However, these small molecules remain in a free state within the polymer matrix, potentially leading to phase separation. Such microstructural instability could interrupt the continuity of ion transport pathways in the host polymer, ultimately degrading overall ionic conductivity. In addition, excess small molecules may induce undesirable side reactions at the lithium metal anode compromising the stability of the solid electrolyte interphase (SEI).

Previous studies have shown that incorporating inorganic active fillers into the polymer matrix is an effective strategy [14,15]. On one hand, the active fillers effectively suppress the crystallization behavior, expanding the amorphous regions and enhancing chain segment mobility, thereby providing a more dynamic environment for Li+ migration. On the other hand, the fillers such as LLZO, LATP, and LLTO exhibit intrinsic Li⁺ conduction and can introduce additional inorganic migration pathways independent of the polymer. This enables multipathway synergistic conduction, reducing the dependence of ion transport on the polymer chain segments [16-18]. For instance, in the PEO-LLZTO system, the incorporation of LLZTO led to an order of magnitude increase in the ionic conductivity compared to the pure PEO [19,20]. However, the enhancement effect of these fillers is strongly influenced by factors such as particle size, morphology, content, and interface properties. Studies have shown that with low filler concentrations, active fillers struggle to establish continuous migration pathways [21,22]. Conversely, elevated concentrations promote particle aggregation, resulting in phase segregation and a concomitant rise in interfacial impedance at organic-inorganic boundaries. Nan et al. revealed that the interfacial interactions of fillers-polymers were in the range of tens of nanometers by AFM-IR [23]. Similarly, Liu et al. utilized ADF-STEM to observe a gradient distribution of Li⁺ concentration across the interfacial region, further corroborating the dynamic ion transport behavior at these interfaces [24]. These findings demonstrate the synergistic role of the filler-polymer interface in enhancing ion conduction within composite polymer electrolytes (CPEs). However, the high interfacial impedance arising from conventional particulate active fillers impedes efficient ion transport across organic-inorganic interfaces, limiting macroscopic-scale conduction in such CPEs [25]. Therefore, although the incorporation of inorganic fillers into SPEs provides

additional ion conduction pathways, many charge carriers remain concentrated in the polymer matrix, limiting the full utilization of Li $^{\rm +}$ conduction characteristics of the active fillers. In some cases, it may only exhibit behavior similar to that of inert fillers, such as SiO $_2$ or Al $_2$ O $_3$. Hence, constructing a percolating dynamic ion-conduction network remains a critical challenge in achieving efficient long-range ion conduction. One-dimensional (1D) nanofillers with high aspect ratios (such as nanowires and nanofibers) can establish long-range percolating networks, creating spatially continuous ion transport pathways across multiple length scales even at low filler loadings [26,27]. Furthermore, the high specific surface area enhances interfacial interactions with polymer chains, promoting the formation of amorphous regions at organic-inorganic interfaces. This structural modification enables Li $^{\rm +}$ to establish continuous and efficient transport pathway through the dynamic chain segments, inorganic fillers and their interfacial regions.

Herein, this study proposes a strategic approach to construct a percolating dynamic ion transport network through the in-situ polymerization of DOL monomers within LLTO nanofiber (LLTO NF) scaffold, successfully fabricating a high-performance PDOL@LLTO composite polymer electrolyte (as in Fig. 1). This approach concurrently incorporates dynamic acceleration of microscopic ion solvation structures and long-range inorganic network-assisted construction of lowcrystalline, continuous, and rapid polymer transport channels, thereby promoting efficient Li⁺ transport across multi-scale architectures. Specifically, the in-situ polymerization of DOL reduces the interfacial contact impedance between PDOL and LLTO NF, generating a chargeenriched organic-inorganic interface which enhances interfacial ion transport kinetics. Meanwhile, residual DOL coordinates with Li significantly weakening the solvation of Li⁺ by PDOL, thus accelerating the desolvation process. Furthermore, the high aspect ratio LLTO NF forms a continuous, permeable 3D inorganic network that constructs low-impedance, multi-scale ion migration channels within the polymer matrix, effectively circumventing the constrained transport pathways inherent to amorphous regions. Through the synergy of the dual mechanisms, PDOL@LLTO overcomes the static ion transport bottleneck commonly observed in SPE, achieving exceptional excellent room temperature ionic conductivity of $1.62 \times 10^{-4} \, \mathrm{S \ cm^{-1}}$ and an outstanding Li^+ transference number ($t_{Li}^+ = 0.61$). Benefiting from the uniform Li^+ flux enabled by PDOL@LLTO, lithium deposition at the anode is significantly stabilized. Moreover, PDOL suppresses DOL decomposition, facilitating the formation of an inorganic-rich SEI, which effectively inhibits the growth of dendrites. Electrochemical evaluation demonstrates outstanding stability, with Li|PDOL@LLTO|Li symmetric cells maintaining stable operation for 1000 h at 0.4 mA cm⁻², and LiFePO₄||Li full cells retaining 94.6 % capacity after 100 cycles at 2C. Additionally, PDOL@LLTO exhibits remarkable high-voltage stability. After 100 cycles, the Li|PDOL@LLTO|NCM811 full cell demonstrates exceptional capacity retention.

2. Result and discussion

Fig. 2a illustrates the fabrication process of PDOL@LLTO CPE. Firstly, LLTO NF were synthesized via sol-gel electrospinning method followed by calcination at 800 °C for 4 h in air. As shown in Fig. 2b, the synthesized LLTO NF features a well-defined 3D interconnected porous network, with an average diameter of approximately 300 nm. TEM image (Fig. 2c) further illustrates that the calcined LLTO NF consists of interconnected LLTO nanoparticles, with coherent grain boundaries that ensure the structural integrity of the material. The high aspect-ratio LLTO NF forms a percolating 3D network that not only provides abundant surface Li⁺ hopping sites but also establishes continuous low-resistance conduction pathways throughout the bulk. Elemental mapping image (Fig. S1) confirms the uniform distribution of La, Ti, and O elements throughout LLTO NF. Secondly, the in-situ ring-open polymerization was achieved by infiltrating the LLTO NF with 1,3-dioxolane (DOL) precursor solution and induced by LiFP₆. It is worth noting that

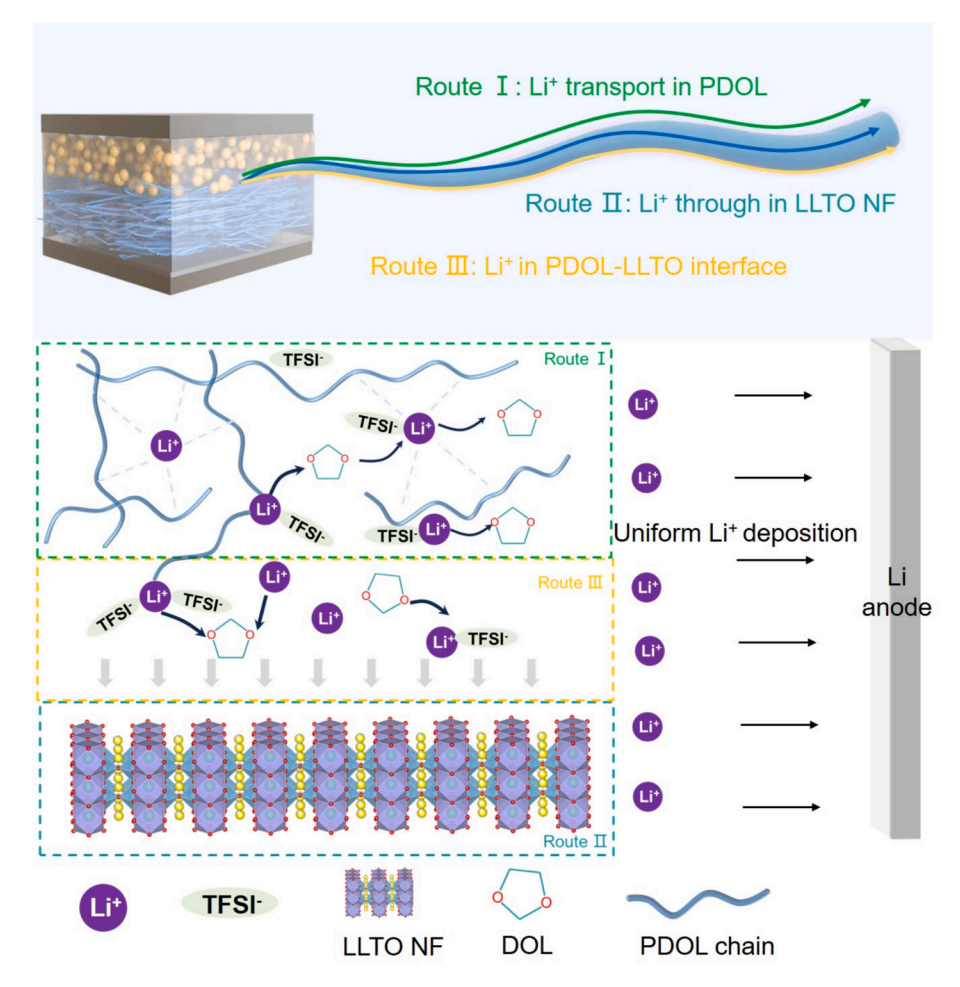


Fig. 1. Schematic diagram of ion transport in PDOL@LLTO, including PDOL, PDOL-LLTO interface with LLTO NF.

this polymerization process is incomplete. Different concentrations of initiators may form different degrees of polymerization. Furthermore, this remaining DOL significantly impact both the crystalline structure of PDOL and the solvation dynamics of Li⁺. As demonstrated by the XRD results (Fig. 2d), no distinct crystalline peaks are observed in PDOL@LLTO, in contrast to PEO (Fig. S2), suggesting that PDOL contributes to a low-crystallinity structure. As illustrated in Fig. 2e, the cross-sectional SEM image of the PDOL@LLTO reveals that the LLTO NF are completely embedded within the PDOL matrix, forming a homogeneous layer with a thickness of approximately 45 μm . And no obvious pores are observed, indicating that the in-situ polymerization of DOL monomers enables tight interfacial coupling between the polymer matrix and the inorganic framework, effectively preventing phase separation and interfacial defects. The intimate interfacial contact suggests effective Li⁺ conduction pathways throughout the entire structure. Fig. 2f shows that PDOL@LLTO exhibits a low glass transition temperature (Tg) of -30.9 °C. Such dynamic flexibility effectively alleviates the structural constraints imposed by the aggregated state on Li⁺ couplingdecoupling kinetics, thereby facilitating improved ion transport. Ionic conductivity serves as a critical performance metric for SPEs, exhibiting pronounced temperature dependence that arises from their semicrystalline nature. Fig. 2g presents the electrochemical AC impedance spectra (EIS) of PDOL@LLTO at different temperatures. It is observed that the impedance exhibits only slight variation with temperature. Moreover, PDOL@LLTO exhibits low impedance at room temperature, corresponding to a high ionic conductivity of $1.62 \times 10^{-4} \text{ S cm}^{-1}$ and low activation energy of 0.10 eV, which is significantly higher than that of both PDOL and PEO (Fig. S3). So, this spatially interconnected architecture establishes a percolating dynamic ion-conduction network in

PDOL@LLTO, effectively eliminating the ion migration barriers and substantially improving the ionic transport behavior.

It also should be pointed out that PDOL is a dual-ion conductor, with both cations and anions contributing to the ionic conductivity. However, in practice, only cations contribute significantly to the ion transport. Particularly at elevated current densities, a high t_{Li} promotes uniform lithium deposition while minimizing the charging/discharging polarization. Therefore, the t_{Li} serves as a key metric for evaluating the contribution of Li⁺ to the overall ionic conductivity. Electrochemical characterization reveals that the PDOL@LLTO CPE achieves a superior t_{Li}^+ of 0.61, representing 2.8 and 4.7 times to pure PDOL (t_{Li}^+ = 0.22) and PEO ($t_{Li}^+ = 0.13$) electrolytes, respectively (Figs. 3a-b, S4). This enhancement can be attributed to the unique spatially interconnected architecture formed through synergistic interactions between PDOL and LLTO components. Firstly, LLTO NF itself exhibits a high theoretical t_{Li}⁺ value, and its spatially interconnected fiber network establishes continuous Li⁺ permeation pathways at the macroscopic level. Secondly, PDOL provides sufficient chain segment mobility and carrier concentration. Moreover, the residual DOL could optimize the solvation structure between Li⁺ and PDOL, thereby accelerating the kinetics of this coordination process thus further improving the t_{Li}⁺. Consequently, under the synergistic effect of structure and composition, the effective lithium ion conductivity (σ_{Li}^+) of PDOL@LLTO is elevated to 0.98×10^{-4} S cm⁻¹, higher than that of PDOL ($\sigma_{Li}^+ = 2.53 \times 10^{-5}$ S cm⁻¹) and PEO $(\sigma_{Li}^+ = 2.17 \times 10^{-7} \text{ S cm}^{-1})$ in Fig. 3c. The electrochemical stability window of the PDOL@LLTO CPE was evaluated using linear sweep voltammetry (LSV). Results demonstrate an extended stability up to 4.3 V vs. Li⁺/Li, representing a significant enhancement compared to conventional PEO-based electrolytes. These results demonstrate that LLTO

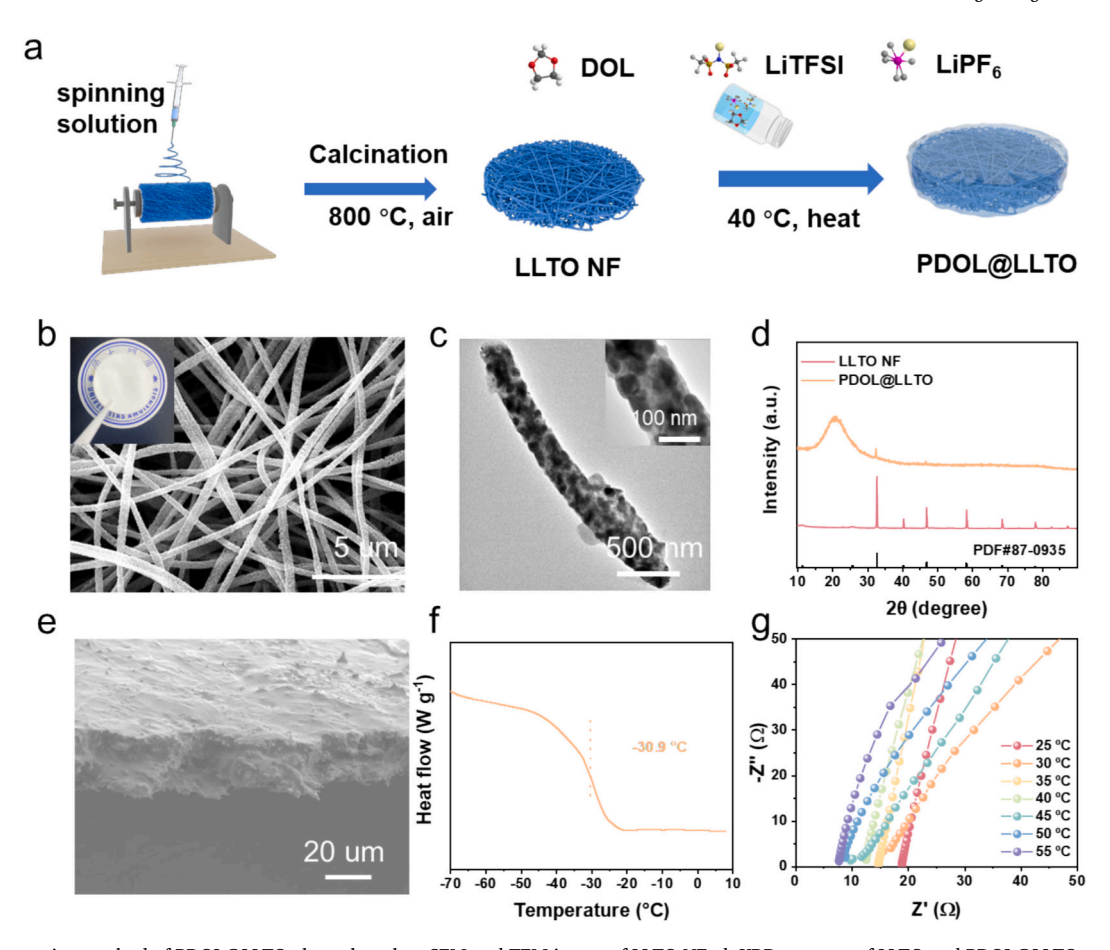


Fig. 2. a, the preparation method of PDOL@LLTO electrolyte. b-c, SEM and TEM image of LLTO NF. d, XRD patterns of LLTO and PDOL@LLTO. e, the cross-section SEM picture of PDOL@LLTO. f, the DSC plot for PDOL@LLTO. g, EIS curve of PDOL@LLTO at different temperatures.

NF serves as an effective stabilizer for polymer chains, while residual DOL from in situ polymerization remains confined within the polymer matrix. This dual mechanism significantly suppresses oxidative decomposition pathways (Fig. 3d). To further assess the interfacial stability of the electrolyte to the Li anode, symmetric Li||Li cells were assembled and electrochemically characterized. As in Fig. 3e, the interfacial impedance of the Li|PDOL@LLTO|Li cell exhibits minimal evolution over 9 days of observation, indicating the high stability of both the electrolyte and the electrode-electrolyte interface.

Considering the favorable electrochemical stability and performance observed in PDOL@LLTO, it is crucial to investigate the underlying mechanisms that govern these behaviors. Specifically, the solvation environment surrounding Li⁺ plays a pivotal role in percolating dynamic ion-conduction network. As above mentioned, the in-situ polymerization process results in residual DOL molecules. The interactions between the solvent molecules (both polymeric PDOL and monomeric DOL) and significantly influence the coordination environment, thereby affecting the ionic transport behavior. In Fig. 3f, density functional theory (DFT) calculations were conducted to assess the contribution of each component to the solvation structure in PDOL, with G5 used as a simplified model for the long PDOL chains. The binding energies of PDOL and DOL to Li^+ were found to be -1.83 eV and -1.75 eV, respectively. Both components exhibit comparable electrostatic potential distributions (Fig. S5), further indicating that DOL possesses a strong affinity for Li⁺. This indicate that remaining DOL in PDOL@LLTO exists not as free molecules, but participates in forming a dynamic Li⁺ solvation structure through synergistic interactions. This unique coordination environment enhances ionic transport while maintaining interfacial stability. This observation is further corroborated by the Raman spectra, as shown in Fig. 3 g. The state of anions within the electrolyte system can

be categorized into three distinct configurations: free anions (FA), contact ion pairs (CIP), and anion aggregates (AGG). [28] The blue shift of the S-N-S stretching vibration (740 to 744 cm⁻¹) from PEO to DOL suggests that the presence of remaining DOL promotes the formation of additional CIP and AGG in the solvated structure. The content of each species was quantified based on the corresponding peak areas, as illustrated in Figs. 3h-i and S6. Due to the strong solvation affection of the long PEO chains, anions are largely excluded from the solvation structures and predominantly remain in a free state (FA = 84.7 %). In contrast, within the DOL solution, solvent molecules, cations and anions collectively participate in coordination, leading to a significantly higher proportion of contact ion pairs (CIP, 26.3 %) and aggregates (AGG, 26.6 %) (Fig. S7). For the PDOL, the presence of abundant CIP (28.3 %) and AGG (18.2 %) creates a more easily decoupled solvation environment. The presence of DOL allows the anion to participate in the formation of the solvated structure and reduces the binding of Li⁺ by the multidentate chelated solvated structure in PDOL. As a result, the desolvation process of Li⁺ is accelerated. The DOL-assisted weak solvation structure establishes low-impedance ion migration pathways within the polymer, alleviating the inherent transport limitations of amorphous regions and enabling dynamic ion percolation throughout the PDOL@LLTO CPE.

The Li plating/stripping behavior at the anode interface plays a critical role in determining long-term cycling stability of the battery system. As shown in Fig. 4a-b, the lithium deposition process was evaluated using Li||Cu cells. Benefiting from both high ionic conductivity and Li $^+$ transference number achieved through the percolating dynamic ion-conduction network structure, the Li|PDOL@LLTO|Cu cell achieves stable cycling for 80 cycles at 0.2 mA cm $^{-2}$, whereas the Li|PDOL|Cu cell displays poor cycling stability. Meanwhile, the excellent Coulombic efficiency of 87.2 % achieved by Li|PDOL@LLTO|Cu cell is

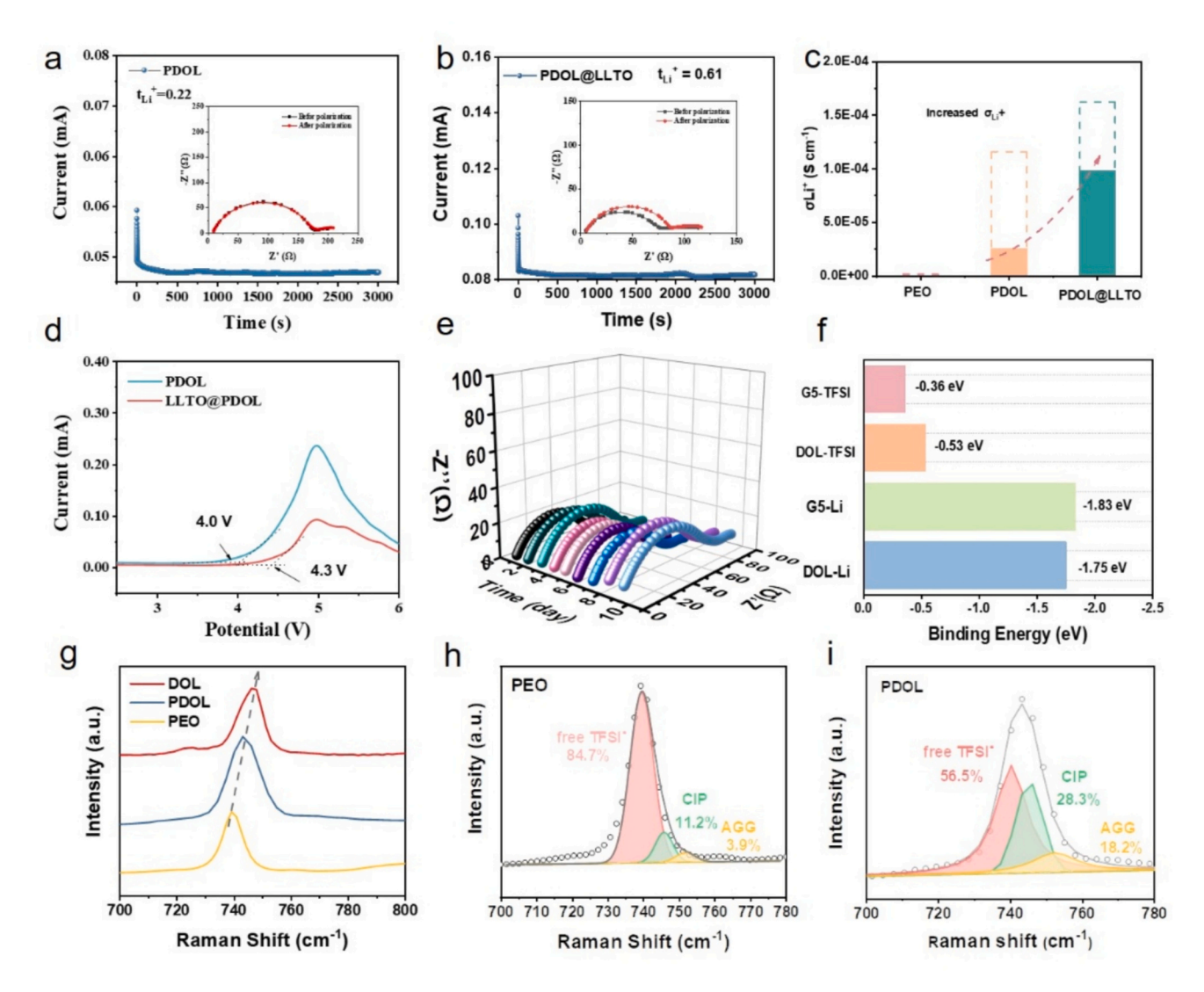


Fig. 3. a-b, Li⁺ transference number for PDOL and PDOL@LLTO. c, Li⁺ contribution to overall ionic conductivity of PEO, PDOL and PDOL@LLTO. d, LSV curves of PDOL and PDOL@LLTO. e, impedance spectra for Li|PDOL@LLTO|Li battery over 9 days. f, binding energies of different solvents with Li⁺ and TFSI⁻. g, vibrations of S-N-S in PEO, DOL and PDOL. h-i, the ion dissociation of LiTFSI in PEO and PDOL.

also closely associated with its high t_{Li} and stable electrode interface. Moreover, the initial Li deposition curve reveals that PDOL@LLTO present a lower and flatter nucleation overpotential of 10.1 mV (< 28.8 mV of PDOL). This indicates the ability to achieve more uniform Li deposition, thereby reducing the risk of dendrite formation. At the same time, the Tafel plot (Fig. 4c) shows that PDOL@LLTO processes an excellent exchange current density of 0.40 mA cm⁻², compared to PDOL of $0.14~\text{mA}~\text{cm}^{-2}$. This suggests the in-situ polymerization strategy enables a rapid Li⁺ plating/stripping kinetics at the electrode-electrolyte interface, thereby suppressing dendrite growth and ensuring excellent cycling stability of the solid-state battery. To determine the critical current density (CCD) of the electrolytes, galvanostatic tests were performed in the range of 0.05–5 mA cm $^{-2}$ in Fig. 4d-e. The potential fluctuations at high current densities are associated with interfacial polarization, suggesting that CCD is primarily governed by uneven Li⁺ flux. Li|PDOL@LLTO|Li cell exhibits a CCD of 3.5 mA cm⁻², a significant improvement compared to that of PDOL (0.5 mA cm⁻²), suggesting enhanced interfacial ion transport kinetics and effective suppression of lithium dendrite formation. The long-term cycling stability of the electrolytes was evaluated through galvanostatic charge-discharge tests, as illustrated in Fig. 4 f-g. While the Li|PEO|Li cell short-circuited after 450 h at 0.2 mA $\text{cm}^{-2},$ both the Li|PDOL|Li and Li|PDOL@LLTO|Li cells

maintained stable operation for over 1000 h. Moreover, PDOL@LLTO exhibited the lowest polarization potential of 30 mV. Notably, the Li PDOL@LLTO|Li cell also achieved stable long-term cycling for over 1000 h at a higher current density of 0.4 mA cm⁻². These results demonstrate that the synergistic organic-inorganic percolating dynamic ion-conduction network in PDOL@LLTO facilitates a uniform Li+ flux within the electrolyte, effectively avoiding ion accumulation. After that, SEM and XPS analyses were performed to investigate the lithium deposition morphology and composition of the lithium foil in the cycled Li||Li cell (cycled at 0.2 mA cm⁻² for 100 h). SEM images (Fig. S8) reveal that after cycling with the PDOL, the Li anode surface displays uneven and block-like Li deposits. While for the PDOL@LLTO, the Li anode surface remains flat and dense. In addition, the evolution of SEI composition plays a pivotal role, as a mechanically stable and chemically inert SEI is crucial for both suppressing lithium dendrite propagation and ensuring interfacial stability with the lithium anode. As shown in Fig. S9, The C 1 s of PDOL includes C-C (284.8 eV), C-O (286.6 eV), C=O (287.8 eV), and C-F (292.8 eV), indicating that the SEI is composed of both organic and inorganic components [29]. Regarding the F 1 s, peaks at 688.6 eV and 684.8 eV correspond to -CF₃ and LiF, respectively [30]. The O 1 s spectrum corresponds to C-O, Li₂CO₃ and C=O species. Generally, organic species in a hybrid SEI can

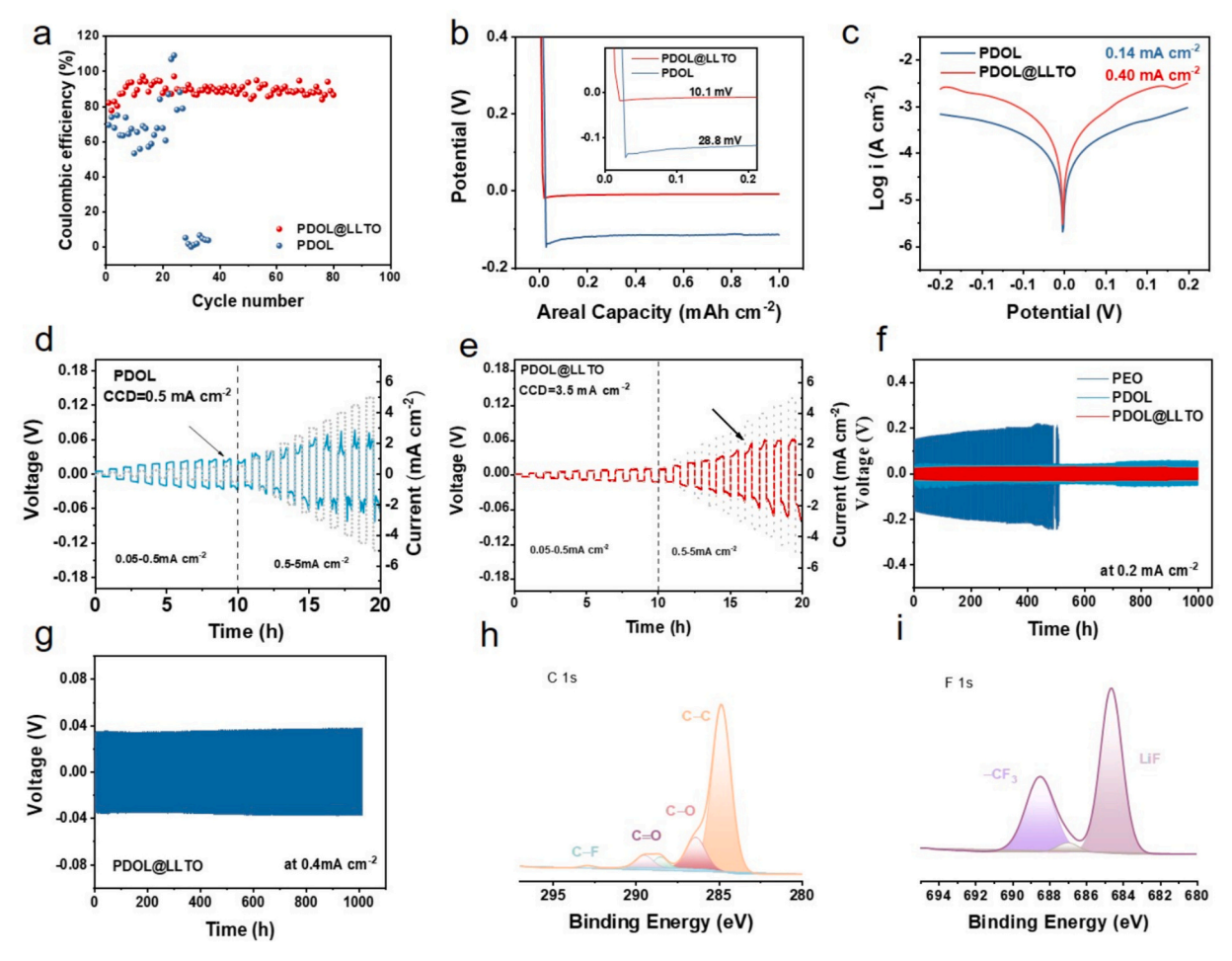


Fig. 4. a-b, the Coulombic efficiency of electrolytes in Li||Cu cells with 1 mAh cm $^{-2}$ at 0.2 mA cm $^{-2}$ and the initial Li plating curves. c, Tafel curves in Li||Li symmetric cells measured at a scan rate of 1 mV s $^{-1}$. d-e, the CCD plots of PDOL and PDOL@LLTO which was carried out at 0.05–5 mA cm $^{-2}$. f, Lithium plating/stripping performance of PEO, PDOL and PDOL@LLTO in Li||Li symmetric cells at 0.2 mA cm $^{-2}$.g, Li|PDOL@LLTO|Li cell measured at 0.4 mA cm $^{-2}$. h-i, XPS profiles with C 1 s and F 1 s of PDOL@LLTO, respectively.

maintain good electrode-electrolyte contact and help reduce interfacial resistance, while inorganic species enhance the mechanical robustness of the SEI, thus constructing a stable interface electrolyte and lithium metal. Compare to PDOL, PDOL@LLTO exhibits an increased proportion of inorganic components such as LiF and $\rm Li_2CO_3$ in the SEI after cycling, which contributed to the formation of a denser SEI inhibiting the growth of dendrites (Figs. 4h-i and S10). This phenomenon can be principally explained by DOL-mediated solvation structure modification, wherein the enhanced formation of AGG and CIP facilitates anion-dominated development of an inorganic-enriched solid electrolyte interphase.

The ring-opening polymerization of DOL is inherently incomplete, resulting in the presence of DOL monomers within the system. In addition to the solvation-structure-induced anion-driven SEI formation, a fundamental understanding of how residual DOL molecules modulate microscopic ion conduction pathways in PDOL@LLTO CPE warrants systematic investigation. Owing to DOL's strong coordination affinity for Li⁺, the impact of these residual molecules on ions transport behavior within the electrolyte is non-negligible. While an excess of monomers can enhance ionic conductivity, it may also cause over-swollen of the polymer chains, thereby disrupting the spatial ion transport pathways and ultimately impairing effective Li⁺ percolation. Therefore, the amount of residual DOL needs to be adjusted by controlling the amount of initiator LiPF₆. Fig. 5a presents the FTIR spectra of DOL ring-opening polymerization initiated by LiPF₆. The results show that as LiPF₆ concentration increases, the C-H out-of-plane bending vibration peak of DOL at 914 cm⁻¹ gradually weakens, while the long-chain -(CH₂) -

vibration peak at 842 cm⁻¹ progressively intensifies, indicating the gradual conversion of cyclic DOL monomers into long-chain polymeric PDOL [31]. However, the persistent vibration at 914 cm⁻¹ confirms the presence of residual DOL within the system. The DOL content was further quantified using NMR results, as shown in Fig. 5b.The proton peaks of DOL at 3.78 ppm (a) and 4.78 ppm (b) were markedly diminished, while two new signals at 3.63 ppm (c) and 4.63 ppm (d) appeared, which were attributed to the proton of the -CH₂-CH₂-O-CH₂-O- within PDOL [31,32]. The ratio of c/a reflect the residual amount of DOL in PDOL after the addition of 1.0 M (25.3 %), 1.2 M (11.2 %), 1.5 M (8.0 %), and 1.8 M (6.9 %) LiPF₆. Furthermore, the molar ratio of residual DOL monomers to Li⁺ was quantified (Li⁺ derived from LiTFSI and LiPF₆), as presented in Fig. 5c. At an initiator concentration of 1.0 M, the molar ratio of DOL to Li⁺ was as high as 1.7, indicating a substantial excess of DOL relative to Li⁺. With increasing initiator concentration, this ratio progressively declined to 0.68, 0.44, and 0.28, respectively. These findings indicate that higher initiator concentrations effectively diminish the dominant role of DOL in regulating Li⁺ transport, thereby optimizing the overall ion transport dynamics within the polymer matrix. The solvation structure of PDOL was investigated using Raman spectroscopy, as depicted in Fig. 5d. The peak at 845 cm⁻¹, attributed to the coupling of C—H and C—O stretching vibrations in PDOL, gradually blue shifted to 848 cm⁻¹ as the amount of LiPF₆ increased. This blue shift is indicative of stronger interchain interactions, implying that the increasing degree of polymerization promotes greater segmental entanglement within the polymer matrix [33]. As a result, the dynamic

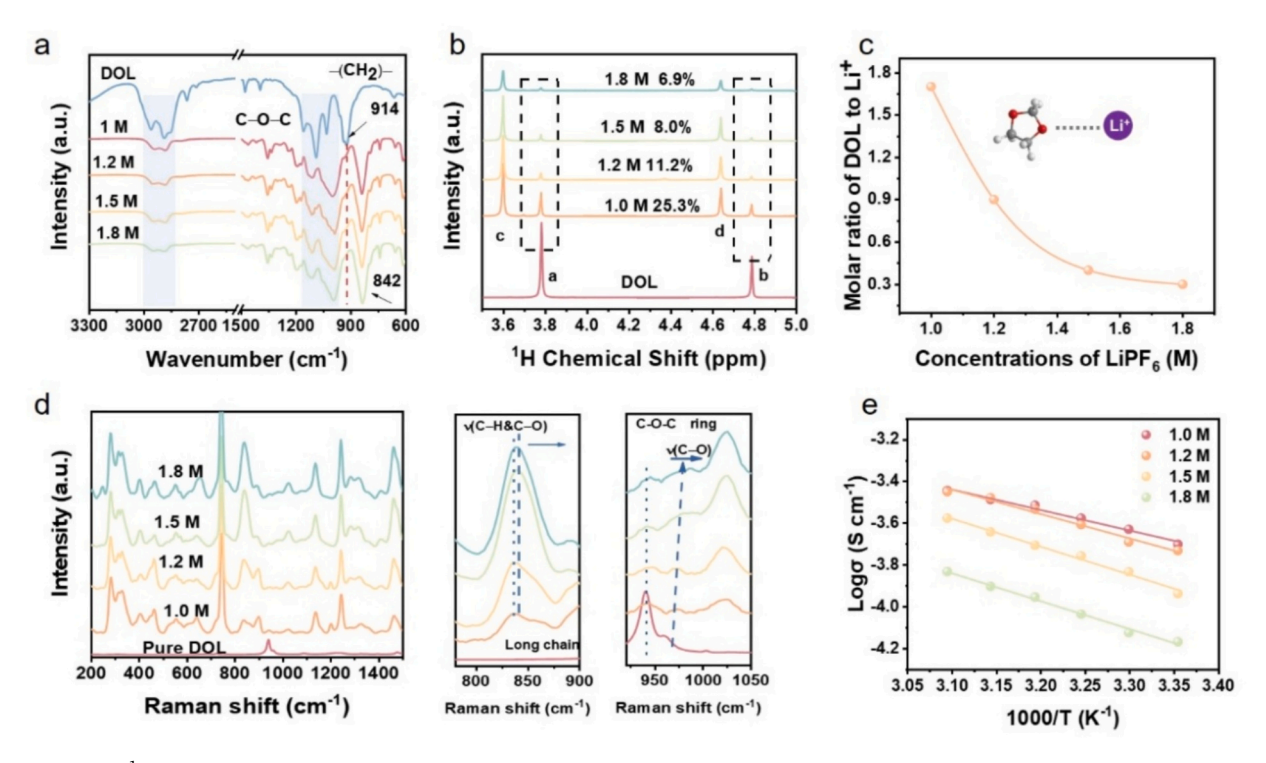


Fig. 5. a-b, FTIR and ¹H NMR spectra of DOL and the PDOL with 1.0 M, 1.2 M, 1.5 M, 1.8 M LiPF₆ concentrations. c, the number of remaining DOL coordinated to Li⁺. d, the Raman plots of DOL and PDOL electrolytes. e, the Arrhenius curves of ionic conductivity for PDOL with different LiPF₆.

capacity of the solvated structure is reduced, which further affects the desolvation process of Li⁺. Meanwhile, 940 cm⁻¹ and 970 cm⁻¹ correspond to free and coordinated DOL. It was observed that the coordinated DOL also exhibits a blue shift, indicating a weak binding interaction between DOL and Li⁺ [34]. The increased degree of polymerization likely facilitates the incorporation of DOL into the Li⁺ coordination structure within PDOL [4,35]. Nevertheless, an excessive presence of residual DOL introduces concerns regarding ion transport efficiency. This inference is further corroborated by variations in ionic conductivity and activation energy, underscoring the critical impact of residual DOL on ion mobility. As shown in Fig. 5e, when the LiPF6 concentration increases from 1.0 M to 1.8 M, the ionic conductivity of PDOL at room temperature decreases from $1.99 \times 10^{-4} \, \mathrm{S \, cm^{-1}}$ to $6.84 \times 10^{-5} \, \mathrm{S \, cm^{-1}}$, while the activation energy (Ea) correspondingly increases from 0.08 eV to 0.11 eV. These results confirm that Li⁺ transport is predominantly mediated by the long-chain PDOL. Therefore, maintaining PDOL as the primary transport framework, while incorporating a moderate amount of DOL molecules, facilitates the formation of a solvation structure with reduced migration energy barriers, thereby enhancing overall ion mobility. Meanwhile, DSC results found that the above PDOL had relatively low Tg values (Fig. S11), which provided a foundation for the dynamic ion transport networks. Thus, rational regulation of the degree of polymerization of DOL and its residual amount is of great significance to achieve the optimal balance between the efficient motility of polymer chain segments and ionic mobility properties. Therefore, to optimize the ionic conductivity and the stability of the ion transport network of the PDOL electrolyte, it is more appropriate to control the content of LiPF₆ at 1.5 M.

Critically, the interfacial properties of the PDOL@LLTO play a pivotal role in facilitating Li⁺ migration across the organic-inorganic interface, which is essential for achieving efficient ion percolation across distinct phases. In this context, the organic-inorganic interface acts as a crucial bridge, linking ion transport within the polymer matrix to that within the inorganic network. To validate the hypothesis that Li⁺ can achieve fully dynamic percolation transport in PDOL@LLTO, it is imperative to elucidate the fundamental role of the interface in bridging

polymer-phase and inorganic-phase ion conduction. The ion diffusion kinetics at the PDOL-LLTO interface was investigated by DFT calculations [36]. Fig. 6a-b analyze the interfacial diffusion kinetics by evaluating the binding energy of the simulated units. The results reveal that the Li⁺ binding energy at the pure LLTO interface is significantly elevated to 3.04 eV, indicating a high diffusion energy barrier that tends to trap Li⁺ at the interface. In contrast, the ion diffusion energy barrier at the PDOL-LLTO interface is reduced by nearly an order of magnitude, decreasing to 0.39 eV. This substantial reduction highlights the critical role of the organic-inorganic interface in facilitating efficient Li⁺ migration across the heterogeneous phases. And PDOL compensates for the physical defects between LLTO particles, facilitating ion migration along the LLTO NF. In addition, differences in the physicochemical properties at the organic-inorganic interface induce charge redistribution, leading to the formation of an internal electric field within the space charge layer (SCL), which further promotes directional ion transport across the interface. According to Chen et al., the formation of a space charge layer (SCL) may be unfavorable for Li⁺ transport, as Li⁺ tends to accumulate within the charge-rich regions of the SCL rather than the charge-depleted areas [37]. In the latter case, the weaker charge compensation effect may lead to stronger electrostatic interactions, further impeding efficient Li⁺ migration. As depicted in Fig. 6c, the charge differential density, where blue and green regions represent electron depletion and accumulation, respectively, reveals a relatively poor initial charge distribution at the PDOL-LLTO interface. This suggests that there remains a certain degree of resistance to achieving seamless synergistic percolation between the organic and inorganic phases, as the diffusion of charge carriers from the polymer matrix into the inorganic surface is hindered. However, the residual DOL molecules retained during the in-situ polymerization of PDOL effectively compensate for this deficiency. The presence of DOL induces a broader electron distribution and enhances electron transfer across the PDOL-LLTO interface, thereby improving interfacial charge uniformity and promoting faster Li+ transport across the interface. Moreover, the chemical environment of Li⁺ was further characterized by ⁷Li NMR (Fig. 6d). Compared with PEO, the ⁷Li chemical position of PDOL with

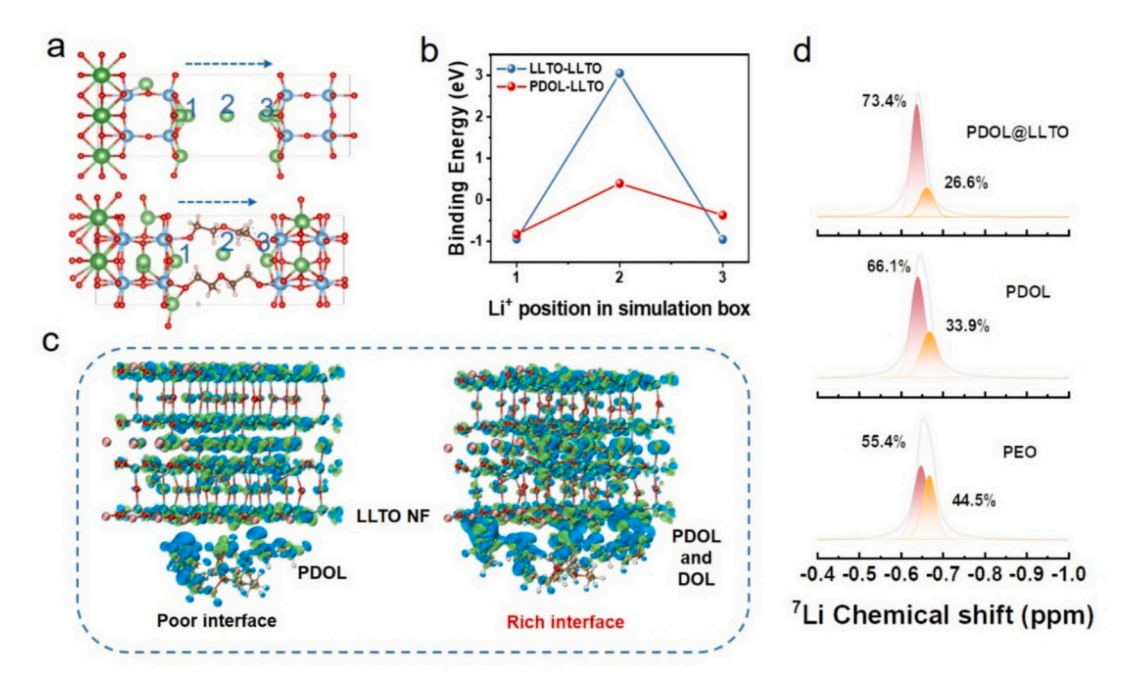


Fig. 6. a, the Li⁺ transport trace at the LLTO-LLTO and PDOL-LLTO interfaces in the DFT simulation box. b, energy barrier for Li⁺ to cross the LLTO-LLTO and PDOL-LLTO interfaces. c, modeling of charge density patterns at PDOL-LLTO and PDOL-LLTO interfaces. d, ⁷Li NMR spectroscopy.

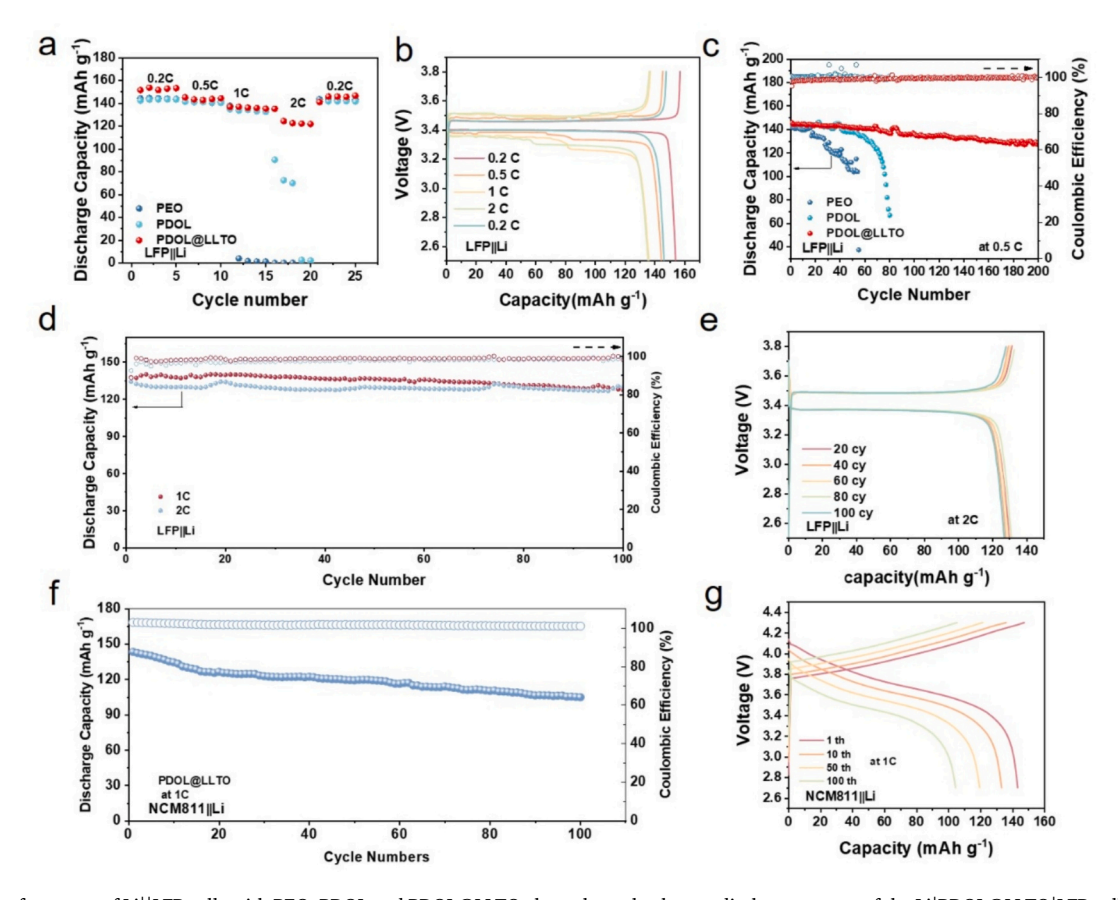


Fig. 7. a, rate performance of Li||LFP cells with PEO, PDOL and PDOL@LLTO electrolytes. b, charge—discharge curves of the Li|PDOL@LLTO|LFP cell at various rates from 0.2C to 2C. c, cycling performance of Li||LFP cells with PEO, PDOL and PDOL@LLTO electrolytes at 0.5C. d, cycling performance of Li||PDOL@LLTO|LFP cell at 1C and 2C. e, charge-discharge curves of the Li||PDOL@LLTO|LFP cell for different cycles at 2C. f-g, the cycling performance and charge-discharge curves of Li||PDOL@LLTO|NCM811 cell at 1C.

PDOL@LLTO is shifted to the lower field, indicating that Li⁺ favors in free state. Peak deconvolution was performed to identify the Li⁺ states, where the right peak (orange region) corresponds to coordinated Li⁺, which contributes less to ionic conductivity. In contrast, the left peak (red region) primarily represents Li⁺ in the weakly bound amorphous region, providing a higher mobility. The results show that the concentration of free Li⁺ in PDOL@LLTO increases to 73.4 %.

To evaluate the electrochemical performance and compatibility of the PDOL@LLTO CPE in practical solid-state battery systems, Li| PDOL@LLTO|LFP full cell was assembled. As shown in Fig. 7a-b, the Li| PDOL@LLTO LFP cell exhibits excellent rate performance compared to Li|PEO|LFP and Li|PDOL|LFP cells, delivering high discharge capacities of 156.9, 151.2, 147.7, and 111.1 mAh g⁻¹ at 0.2C, 0.5C, 1C, and 2C, respectively. The cell capacity could be recovered after the rate performance returned from 2C to 0.2C, indicating a reversible rate capability. After 200 cycles at 0.5C, Li|PDOL@LLTO|LFP maintains 87.5 % of the initial capacity (Fig. 7c). In contrast, the Li|PEO|LFP and Li|PDOL| LFP cells exhibited significant capacity fading, ultimately failing within 60 and 80 cycles, respectively. The results can be attributed to the slow ion transport kinetics in PEO and PDOL, leading to uneven lithium deposition and eventual dendrite penetration that triggers the short circuit of the cells. The cycling stability of Li|PDOL@LLTO|LFP was tested under higher current conditions in Fig. 7d. After 100 cycles at 1C and 2C, it exhibited similar retention rates of 93.7 % and 94.6 %, respectively. The charge-discharge curves with 2C showed a smooth charge/discharge plateau with 0.12 V polarization potential (Fig. 7e). The excellent electrochemical performance of Li|PDOL@LLTO|LFP results from the long-range continuous ion transport network provided by LLTO NF and the low ion transport impedance between PDOL and LLTO NF. To further evaluate the high-voltage stability of the PDOL@LLTO CPE, Li|PDOL@LLTO|NCM811 full cells were assembled and tested under high current density of 1C (Fig. 7f-g). The cell delivered an initial discharge capacity of 143 mAh g⁻¹, indicating efficient lithium-ion transport and stable interfacial compatibility with the high-voltage NCM811 cathode. After 100 cycles, a discharge capacity of 104 mAh g⁻¹ was maintained, corresponding to a capacity retention of 72 %, thereby confirming the structural robustness and electrochemical stability of the PDOL@LLTO electrolyte under extended high-voltage operations.

3. Conclusions

This work proposes a strategy to enhance ion transport in SPEs by constructing a percolating dynamic ion conduction network. Specifically, DOL monomers were in-situ polymerized within the threedimensional LLTO NF scaffold, giving rise to a PDOL@LLTO CPE featuring a spatially interconnected architecture. On one hand, the highaspect-ratio LLTO nanofibers construct a continuous and interconnected 3D inorganic ion-conducting network, providing long-range, lowimpedance pathways for Li⁺ migration. The large specific surface area significantly expands the organic-inorganic interfacial region, facilitating the formation of a stable, ion-rich interface. Moreover, in-situ polymerization of DOL within the LLTO NF effectively reduces the interfacial resistance, laying the structural foundation for a spatially interconnected ion transport network. Owing to these synergistic effects, PDOL@LLTO achieves a remarkable room-temperature ionic conductivity of $1.62 \times 10^{-4} \, \mathrm{S \ cm^{-1}}$ and a low activation energy of 0.10 eV. On the other hand, a small amount of residual DOL participates in the solvation structure with Li⁺, effectively weakening the strong coordination between Li^+ and the polymer chains. This modulation facilitates the decoupling of Li+ from the polymer backbone and promotes its migration within the polymer matrix. Benefiting from this multi-scale synergistic regulation strategy, t_{Li} of PDOL@LLTO is significantly improved to 0.61, demonstrating excellent ion transport capability and interfacial stability. XPS analysis further reveals that PDOL@LLTO forms an SEI layer enriched with inorganic components, effectively suppressing lithium dendrite growth and enhancing interfacial stability at the Li metal anode. Therefore, the assembled lithium symmetric cell was able to stabilize lithium plating and stripping at 0.4 mA cm $^{-2}$ for 1000 h. Despite the high-rate condition of 2C, Li|PDOL@LLTO|LFP cell exhibits a high-capacity retention of 94.6 % after 100 cycles.

CRediT authorship contribution statement

Xueying Yang: Writing — original draft, Investigation, Formal analysis, Data curation, Conceptualization. Chenxi Sun: Writing — original draft, Software. Ruiyang Li: Investigation, Formal analysis. Nanbiao Pei: Writing — original draft, Investigation, Formal analysis. Xinyu Li: Investigation, Formal analysis, Conceptualization. Yi Deng: Investigation, Data curation, Conceptualization. Peng Zhang: Writing — review & editing, Writing — original draft, Supervision, Funding acquisition, Formal analysis. Jie Lin: Writing — review & editing, Supervision, Funding acquisition, Conceptualization. Jinbao Zhao: Writing — review & editing, Writing — original draft, Funding acquisition.

Experiment section

The specific experimental information is provided in the supplementary material.

Declaration of competing interest

The authors declare that they have no known competing financial interests or personal relationships that could have appeared to influence the work reported in this paper.

Acknowledgements

The authors gratefully acknowledge the financial support from National Key Research and Development Program of China [Grant Number 2021YFB2400300], the National Natural Science Foundation of China [No. 21875198, 21875195, 22021001], the Fundamental Research Funds for the Central Universities [20720190040], Royal Society International Exchanges Program [IEC\NSFC\233361], and Northern Ireland Department for the Economy Net-Zero Impact Accelerator.

Appendix A. Supplementary data

Supplementary data to this article can be found online at https://doi.org/10.1016/j.cej.2025.165754.

Data availability

Data will be made available on request.

References

- [1] D. Wang, W. Wang, K. Li, J. Song, X. Yuan, Q. Huang, Z. Tang, L. Fu, Y. Wu, Low-temperature tolerant lithium-rich manganese-based cathode enabled by facile SnO₂ decoration, J. Mater. Chem. A 12 (24) (2024) 14467–14478, https://doi.org/10.1039/d4ta01971g.
- [2] K. Zhou, M. Zhang, X. Zhang, T. Wang, H. Wang, Z. Wang, X. Tang, M. Bai, S. Li, Z. Wang, Y. Ma, A cellulose reinforced polymer composite electrolyte for the wide-temperature-range solid lithium batteries, Chem. Eng. J. 464 (2023), https://doi.org/10.1016/j.cej.2023.142537.
- [3] Y. Wang, G. Wang, P. He, J. Hu, J. Jiang, L.-Z. Fan, Sandwich structured NASICONtype electrolyte matched with sulfurized polyacrylonitrile cathode for high performance solid-state lithium-sulfur batteries, Chem. Eng. J. 393 (2020), https:// doi.org/10.1016/j.cej.2020.124705.
- [4] L. Wang, H. Shi, Y. Xie, Z.S. Wu, Fluorinated boron nitride nanosheet enhanced ultrathin and conductive polymer electrolyte for high-rate solid-state lithium metal batteries, Interdiscip. Mater. 2 (5) (2023) 789–799, https://doi.org/10.1002/ idm2.12121.
- [5] T. Lyu, F. Luo, L. Liang, D. Wang, L. Tao, Z. Zheng, Interfacial chemistry Design for Hybrid Lithium-ion/metal batteries under extreme conditions, Adv. Energy Mater. 14 (29) (2024), https://doi.org/10.1002/aenm.202304520.

- [6] R. Chang, Y. Liu, Y. Zhang, Y. Shi, J. Tang, Z.L. Xu, X. Zhou, J. Yang, Weakening Lithium-ion coordination in poly(ethylene oxide)-based solid polymer electrolytes for high performance solid-state batteries, Adv. Energy Mater. (2025), https://doi. org/10.1002/aepm.202405906
- [7] C. Shen, W. Feng, Y. Yu, H. Wang, Y. Cheng, C. Dong, J. Gu, A. Zheng, X. Liao, X. Xu, L. Mai, In situ polymerization inhibiting Electron localization in hybrid electrolyte for room-temperature solid-state Lithium metal batteries, Adv. Energy Mater. 14 (20) (2024), https://doi.org/10.1002/aenm.202304511.
- [8] L. Zhang, S. Cao, Y. Zhang, C. Zhang, P. Guo, J. Song, Z. Jiang, C. Shi, Regulating lithium-ion transport route via adjusting lithium-ion affinity in solid polymer electrolyte, Chem. Eng. J. 479 (2024), https://doi.org/10.1016/j.cej.2023.147764.
- [9] C.Y. Son, Z.-G. Wang, Ion transport in small-molecule and polymer electrolytes, J. Chem. Phys. 153 (10) (2020), https://doi.org/10.1063/5.0016163.
- [10] X. Yang, J. Liu, N. Pei, Z. Chen, R. Li, L. Fu, P. Zhang, J. Zhao, The critical role of fillers in composite polymer electrolytes for Lithium battery, Nanomicro Lett. 15 (1) (2023) 74, https://doi.org/10.1007/s40820-023-01051-3.
- [11] H.Y. Zhou, Y. Ou, S.S. Yan, J. Xie, P. Zhou, L. Wan, Z.A. Xu, F.X. Liu, W.L. Zhang, Y. C. Xia, K. Liu, Supramolecular polymer ion conductor with weakened Li ion solvation enables room temperature all-solid-state Lithium metal batteries, Angew. Chem. Int. Ed. 62 (35) (2023), https://doi.org/10.1002/anie.202306948.
- [12] R. Fang, B. Xu, N.S. Grundish, Y. Xia, Y. Li, C. Lu, Y. Liu, N. Wu, J.B. Goodenough, Li₂S₆ -integrated PEO-based polymer electrolytes for all-solid-state Lithium-metal batteries, Angew. Chem. Int. Ed. Eng. 60 (32) (2021) 17701–17706, https://doi. org/10.1002/anje.2021.06039
- [13] Y.F. Huang, J.P. Zeng, S.F. Li, C. Dai, J.F. Liu, C. Liu, Y.B. He, Conformational regulation of dielectric poly(Vinylidene fluoride)-based solid-state electrolytes for efficient Lithium salt dissociation and Lithium-ion transportation, Adv. Energy Mater. 13 (15) (2023), https://doi.org/10.1002/aenm.202203888.
- [14] Q. Zhou, X. Yang, X. Xiong, Q. Zhang, B. Peng, Y. Chen, Z. Wang, L. Fu, Y. Wu, A solid electrolyte based on electrochemical active Li₄Ti₅O₁₂ with PVDF for solid state Lithium metal battery, Adv. Energy Mater. 12 (39) (2022), https://doi.org/ 10.1002/aenm.202201991.
- [15] P. Zhai, Z. Yang, Y. Wei, X. Guo, Y. Gong, Two-dimensional fluorinated graphene reinforced solid polymer electrolytes for high-performance solid-state Lithium batteries, Adv. Energy Mater. 12 (42) (2022), https://doi.org/10.1002/ aepm.202200967.
- [16] C. Bao, C. Zheng, M. Wu, Y. Zhang, J. Jin, H. Chen, Z. Wen, 12 μm-thick sintered garnet ceramic skeleton enabling high-energy-density solid-state Lithium metal batteries, Adv. Energy Mater. 13 (13) (2023), https://doi.org/10.1002/ aepm 202204028
- [17] K. Jun, Y. Chen, G. Wei, X. Yang, G. Ceder, Diffusion mechanisms of fast lithiumion conductors, Nat. Rev. Mater. (2024), https://doi.org/10.1038/s41578-024-00715-9
- [18] S. Li, J. Lu, Z. Geng, Y. Chen, X. Yu, M. He, H. Li, Solid polymer electrolyte reinforced with a Li_{1.3}Al_{0.3}Ti_{1.7}(PO₄)₃-coated separator for all-solid-state Lithium batteries, ACS Appl. Mater. Interfaces 14 (1) (2022) 1195–1202, https://doi.org/ 10.1021/acsami.1c21804.
- [19] C. He, H. Ying, L. Cai, H. Chen, Z. Xu, S. Liu, P. Huang, H. Zhang, W. Song, J. Zhang, L. Shi, W. Gao, D. Li, W.Q. Han, Tailoring stable PEO-based electrolyte/ electrodes interfaces via molecular coordination regulating enables 4.5 V solidstate Lithium metal batteries, Adv. Funct. Mater. 34 (51) (2024), https://doi.org/ 10.1002/adfm.202410350.
- [20] Y. Zhang, X. Yu, X. Li, J. Ren, P. He, C. Zhang, C. Teng, Y.-E. Miao, T. Liu, LLZTO crosslinks form a highly stretchable self-healing network for fast healable all-solid lithium metal batteries, Chem. Eng. J. 497 (2024), https://doi.org/10.1016/j.cei.2024.154397.
- [21] X. Mao, Y. Zou, F. Xu, L. Sun, H. Chu, H. Zhang, J. Zhang, C. Xiang, Three-dimensional self-supporting Ti₃C₂ with MoS₂ and Cu₂O nanocrystals for high-performance flexible supercapacitors, ACS Appl. Mater. Interfaces 13 (19) (2021) 22664–22675, https://doi.org/10.1021/acsami.1c05231.
- [22] J. Hou, W. Xie, L. Shang, S. Wu, Y. Cui, Y. Li, Z. Yan, K. Zhang, Y. Lu, J. Chen, Nanocrystals with aggregate anionic structure enable ion transport decoupling of

- chain segment movement in poly(ethylene oxide) electrolytes, Angew. Chem. Int. Ed. (2025). https://doi.org/10.1002/anie.202418783.
- [23] X. Li, S. He, Y. Jiang, J. Wang, Y. Yu, X. Liu, F. Zhu, Y. Xie, Y. Li, C. Ma, Z. Shen, B. Li, Y. Shen, X. Zhang, S. Zhang, C.-W. Nan, Unraveling bilayer interfacial features and their effects in polar polymer nanocomposites, Nat. Commun. 14 (1) (2023), https://doi.org/10.1038/s41467-023-41479-0.
- [24] Y. Liu, R. Hu, D. Zhang, J. Liu, F. Liu, J. Cui, Z. Lin, J. Wu, M. Zhu, Constructing Lirich artificial SEI layer in alloy-polymer composite electrolyte to achieve high ionic conductivity for all solid-state Lithium metal batteries, Adv. Mater. 33 (11) (2021), https://doi.org/10.1002/adma.202004711.
- [25] S.C. Sand, J.L.M. Rupp, B. Yildiz, A critical review on Li-ion transport, chemistry and structure of ceramic–polymer composite electrolytes for solid state batteries, Chem. Soc. Rev. 54 (1) (2025) 178–200, https://doi.org/10.1039/d4cs00214h.
- [26] S. Wang, Y. Zou, F. Xu, C. Xiang, H. Peng, J. Zhang, L. Sun, Morphological control and electrochemical performance of NiCo₂O₄@NiCo layered double hydroxide as an electrode for supercapacitors, J. Energy Storage 41 (2021), https://doi.org/ 10.1016/j.est.2021.102862.
- [27] W. Wang, Y. Yang, J. Yang, J. Zhang, Neuron-like silicone Nanofilaments@ montmorillonite Nanofillers of PEO-based solid-state electrolytes for Lithium metal batteries with wide operation temperature, Angew. Chem. Int. Ed. 63 (34) (2024), https://doi.org/10.1002/anie.202400091.
- [28] Y. Zhu, Z. Lao, M. Zhang, T. Hou, X. Xiao, Z. Piao, G. Lu, Z. Han, R. Gao, L. Nie, X. Wu, Y. Song, C. Ji, J. Wang, G. Zhou, A locally solvent-tethered polymer electrolyte for long-life lithium metal batteries, Nat. Commun. 15 (1) (2024), https://doi.org/10.1038/s41467-024-48078-7.
- [29] P. Lai, X. Deng, Y. Zhang, J. Li, H. Hua, B. Huang, P. Zhang, J. Zhao, Bifunctional localized high-concentration electrolyte for the fast kinetics of Lithium batteries at low temperatures, ACS Appl. Mater. Interfaces 15 (25) (2023) 31020–31031, https://doi.org/10.1021/acsami.3c04747.
- [30] S. Liu, M. Liu, L. Du, H. Song, Z. Cui, Engineering ion conduction Nanodomain spacing and Interface environment for Ultrastable all-solid-state Lithium metal batteries, Adv. Funct. Mater. 34 (33) (2024), https://doi.org/10.1002/ adfp. 202400333
- [31] J. Ma, X. Feng, Y. Wu, Y. Wang, P. Liu, K. Shang, H. Jiang, X. Hou, D. Mitlin, H. Xiang, Stable sodium anodes for sodium metal batteries (SMBs) enabled by insitu formed quasi solid-state polymer electrolyte, J. Energy Chem. 77 (2023) 290–299, https://doi.org/10.1016/j.jechem.2022.09.040.
- [32] Y. Liu, Y. Xu, Porous membrane host-derived in-situ polymer electrolytes with double-stabilized electrode interface enable long cycling lithium metal batteries, Chem. Eng. J. 433 (2022), https://doi.org/10.1016/j.cej.2021.134471.
- [33] Y. Wang, T. Li, X. Yang, Q. Yin, S. Wang, H. Zhang, X. Li, 2D solid-electrolyte interphase built by high-concentration polymer electrolyte for highly reversible silicon anodes, Adv. Energy Mater. 14 (2) (2023), https://doi.org/10.1002/ aemm 202303189
- [34] H. Fu, X. Ye, Y. Zhang, Y. Zhong, X. Wang, C. Gu, J. Tu, Toward ultralow temperature Lithium metal batteries: advancing the feasibility of 1,3-Dioxolane based localized high-concentration electrolytes via Lithium nitrate, Adv. Energy Mater. 14 (39) (2024), https://doi.org/10.1002/aenm.202401961.
- [35] J. Atik, D. Diddens, J.H. Thienenkamp, G. Brunklaus, M. Winter, E. Paillard, Cation-assisted Lithium-ion transport for high-performance PEO-based ternary solid polymer electrolytes, Angew. Chem. Int. Ed. 60 (21) (2021) 11919–11927, https://doi.org/10.1002/anie.202016716.
- [36] J. VandeVondele, M. Krack, F. Mohamed, M. Parrinello, T. Chassaing, J. Hutter, Quickstep: fast and accurate density functional calculations using a mixed Gaussian and plane waves approach, Comput. Phys. Commun. 167 (2) (2005) 103–128, https://doi.org/10.1016/j.cpc.2004.12.014.
- [37] Z. Cheng, M. Liu, S. Ganapathy, C. Li, Z. Li, X. Zhang, P. He, H. Zhou, M. Wagemaker, Revealing the impact of space-charge layers on the Li-ion transport in all-solid-state batteries, Joule 4 (6) (2020) 1311–1323, https://doi.org/ 10.1016/j.joule.2020.04.002.